Abdominal Vessels

9

Justin Barr and Sara K. Rasmussen

Abdominal Vessel Anatomy

Every abdominal organ and its vascular supply can be assessed using ultrasound. Color and spectral Doppler can be employed to measure flow characteristics and detect or monitor pathologies or postoperative results.

The aorta supplies arterial blood to the abdominal viscera and has several feeding vessels supplying the structures in the abdomen. The first major trunk is the celiac artery, which usually gives rise to the left gastric, splenic, and common hepatic arteries, although there is wide anatomic variation (Fig. 9.1a, b). The common hepatic artery gives off the right gastric artery and the gastroduodenal artery before it becomes the proper hepatic artery. It then divides into the left and right hepatic branches. The cystic artery commonly branches off the right hepatic artery. The gastroduodenal artery gives rise to the supraduodenal artery, the right gastroepiploic artery, and the superior pancreaticoduodenal artery. The right and left gastric arteries join along the lesser curve of the stomach. The splenic artery gives rise to the short gastric arteries and the left gastroepiploic arteries that supply the stomach.

The superior mesenteric artery (SMA) is the next major trunk off the aorta (Fig. 9.2a, b). This artery supplies the midgut with blood. The SMA first gives rise to the middle colic artery and then the right colic artery as well as the ileocolic artery. The SMA also gives rise to the several arcuate arteries that provide most of the blood to the small intestine. The middle colic artery gives rise to the marginal artery of Drummond, which supplies the transverse and the left colon.

The left and right renal arteries also originate from the aorta, most commonly inferior to the SMA and superior to the inferior mesenteric artery (IMA), though there is wide anatomic variation here as well. Most often the renal arteries are single, but they can be double or have early and varied branching. The adrenal glands receive their blood supply from suprarenal arteries that branch directly off of the aorta as well, usually superior to the main renal arteries.

Inferior to the SMA are the gonadal arteries, which supply the testicle or ovary, and the IMA. The IMA arises proximal to the bifurcation of the aorta. The main branches of the IMA are the left colic artery, which anastomoses with the aforementioned marginal artery of Drummond, and the colosigmoid artery. Distal to the take off of the colosigmoid is the origin of the rectosigmoid artery. The superior rectal arteries are the final branches of the IMA.

S. K. Rasmussen (✉) · J. Barr
Department of Surgery, University of Virginia,
P.O. Box 800709, 1215 Lee Street, Charlottesville,
VA 22908, USA
e-mail: Skr3f@virginia.edu

J. Barr
e-mail: jnb9k@virginia.edu

S. Scholz, M. D. Jarboe (eds.), *Diagnostic and Interventional Ultrasound in Pediatrics and Pediatric Surgery,* DOI 10.1007/978-3-319-21699-7_9

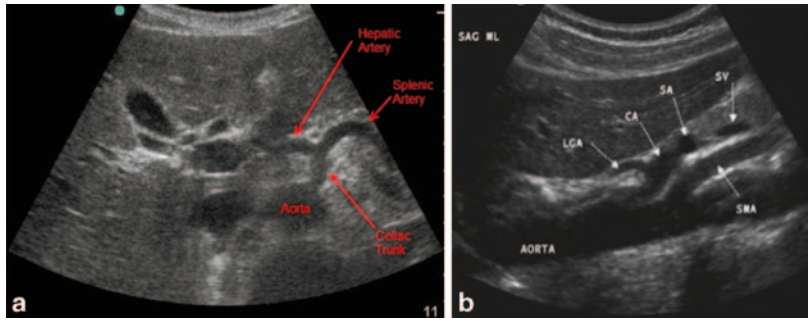

Fig. 9.1 **a** During sonography, look for the vertebral body in the transverse plane. The aorta and inferior vena cava *(IVC)* will be anterior to it. The *IVC* is compressible. The aorta will be anechoic with a pulsating circle. In the proximal aorta, the celiac trunk can be seen with its branches (seagull sign—hepatic and splenic arteries are the wings). **b** Sagittal epigastric view of the aorta and its branches, celiac artery *(CA)*, splenic artery *(SA)*, left gastric artery *(LGA)*, and the superior mesenteric artery *(SMA)*. The splenic vein *(SV)* is visualized below the transverse cut of the pancreas (https://carmenwiki.osu.edu/display/10337/AAA)

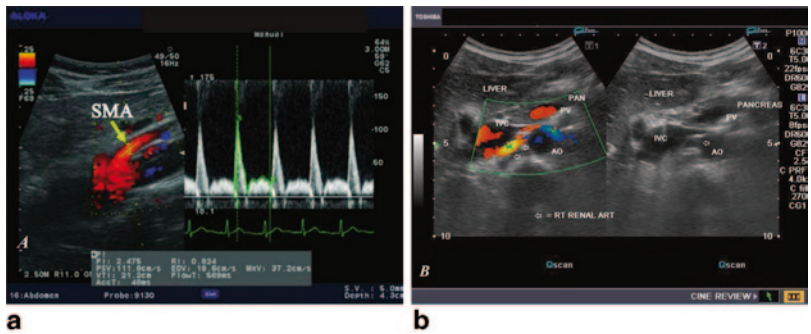

Fig. 9.2 **a** Color Doppler image of the aorta and the *SMA*. **b** *Grayscale* and color Doppler images show the origin of the normal right renal artery from the abdominal aorta *(Ao)*, just below the origin of the superior mesenteric artery. It takes careful adjustment of the wall filter settings to remove the motion artifacts from the aortic pulsations, with appropriate pulse repetition frequency (PRF) settings to get a good color flow image of the right renal artery. The right renal artery is seen coursing behind the *IVC* after an antero-lateral origin from the aorta *(Ao)*. The left renal vein *(LRV)* is also seen traversing anterior to the abdominal *Ao* and between it and the *SMA*. The above images are transverse sections through the epigastrium. The liver provides a good window to view these vessels (http://www.ultrasound-images.com/vascular.htm)

The main venous drainage systems of the abdomen are the inferior vena cava (IVC) and portal vein (PV). The superior and inferior mesenteric veins drain the intestines; the superior mesenteric vein (SMV) merges with the splenic vein to form the PV. This confluence usually occurs just dorsal to the pancreas. The gonadal veins have an asymmetric drainage, with the left gonadal vein draining into the left renal vein (LRV) and the right gonadal vein draining into the IVC directly. Similarly, the left suprarenal vein drains into the LRV, and the right suprarenal vein drains directly into the IVC above the renal veins.

Scanning Technique

For best results, exams should be done in the morning when possible. The patient should not have eaten since the previous midnight and refrain from chewing gum to reduce the amount

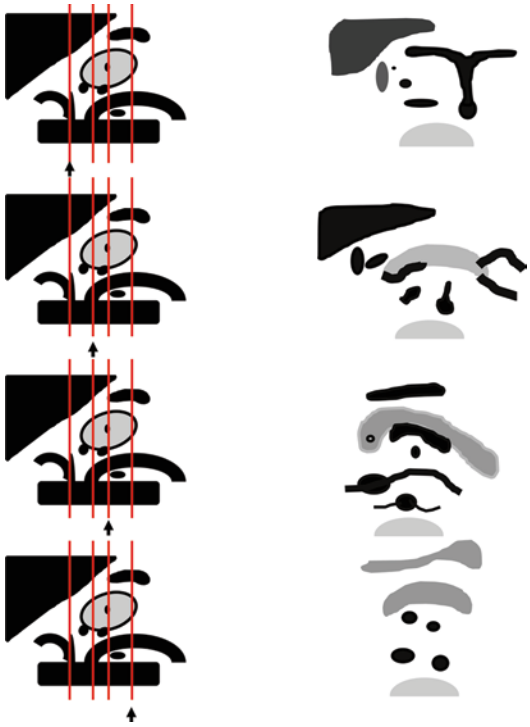

Fig. 9.3 Schematic representation of the abdominal vessels and their relationships to abdominal viscera. *Left*: Sagittal view of abdominal aorta, celiac, *SMA*, and renal artery origins and the pancreas, liver, and spleen with splenic artery and vein. *Right*: Each panel from top to bottom corresponds with a schematic of the ultrasound images that would be seen with the probe positioned in the line marked with the *arrow* in the *left* panel

of gaseous distention of the intestine, which can limit ultrasonography of the abdominal vessels. To reduce bowel gas further, the patient can be asked to drink some water immediately prior to the exam.

Abdominal vessels are typically imaged in several planes (Fig. 9.3). By switching the orientation of the probe, it is possible to measure the diameter of the vessels, the origin of vessels, and their angles as they take off from the abdominal aorta. Use of pulse-wave and color Doppler ultrasound allows measurement of flow in the vessels, with the measurement of velocity, resistive index, and turbuluence of flow. Color Doppler waveforms can provide information about the direction and quality of blood flow through the vessels. Waveforms can distinguish between the arterial and venous blood flow.

Malrotation and Midgut Volvulus

Intestinal malrotation refers to the incomplete rotation of the small intestine in utero. It can result in midgut volvulus, or the complete torsion of the small bowel around the SMA axis, causing acute obstruction requiring prompt surgical intervention. Early recognition of symptoms—bilious emesis—and appropriate, prompt imaging can lead to earlier diagnosis and operation, improving outcomes. The anatomical repositioning of the SMA and SMV during malrotation lends itself to sonographic and especially Doppler diagnosis. Normally, the SMV lies right and ventral to the SMA; in malrotation, that positioning is switched. A large study of 337 patients demonstrated that left/right reversal had a higher sensitivity and specificity for malrotation than ventral/dorsal switching [1–6]. It is possible to have malrotation of the intestines without SMA/SMV reversal, and SMA/SMV reversal can exist without malrotation. In addition this SMA/SMV reversal can be persistent after a Ladd's procedure [7, 8]. The best early study, a prospective comparison of US versus UGI in 427 children, found SMA/SMV reversal to have a 70% sensitivity, 96% specificity, 62% positive predictive value, and 97% negative predictive value [9].

An additional sonographic sign consistent with malrotation is the "Whirlpool sign" [10]. This finding reflects the clockwise rotation of the SMV around the SMA axis as a part of the malrotation. A subsequent study confirmed both the importance of the clockwise orientation (with counterclockwise orientation commonly reflecting nonspecific hemorrhagic enteritis) and the value of this finding [11]. Early reports documented sensitives in the 90th percentiles and specificities approaching 100% [12, 13]. While specificities remain high, reports of whirlpool sign in patients without malrotation have also emerged [14]. Figure 9.4 contains an example illustration [15].

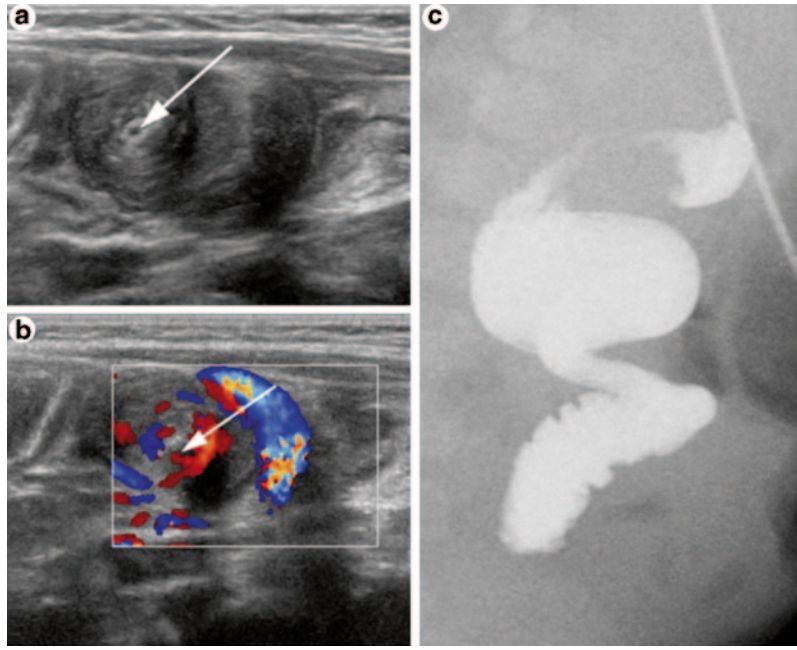

Fig. 9.4 Midgut volvulus diagnosed using ultrasound *(US)* in an 83-day-old boy evaluated for hypertrophic pyloric stenosis. Gray-scale (**a**) and Doppler US (**b**) demonstrate the "whirlpool sign" of the peripheral swirling superior mesenteric vein *(SMV)* around the *SMA* (*arrow*). *UGIs* (**c**), which followed the US, shows the corkscrew sign of midgut volvulus, which was confirmed during surgery [15]

An alternative strategy for diagnosing malrotation with ultrasound involves assessing the position of the third portion of the duodenum (D3). Normally, D3 rests in the retroperitoneum. In malrotation, D3 will be intraperitoneal and anterior to the mesenteric vessels [16]. Sonographic demonstration of a retroperitoneal D3 effectively excludes the diagnosis of malrotation and thus that of midgut volvulus [17–19]. This technique is simple and efficient for diagnosis of malroatation in newborns.

Ultrasound has some limitations. Bowel gas can be problematic. Most series report an inability to perform sonography on around 15% of the patients due to bowel gas interference [20]. Multiple studies have demonstrated a significant false-negative rate with ultrasound, corresponding to sensitivities in the 70–80% range [21]. Given these detractions and the serious consequences of a volvulus diagnosis, clinicians strongly suspicious of malrotation with volvulus should continue to order upper gastrointestinal radiological studies (UGIs), even after a negative ultrasound. However, the low-cost, noninvasiveness, lack of radiation, and strong specificity of several sonographic features—especially whirlpool sign—make ultrasound an excellent screening modality where positive findings may allow the surgeon to skip additional diagnostic steps and proceed directly to the operating room.

Compression Syndromes

Compression syndromes are products of anatomic variants in abdominal vasculature that result in compression of intra-abdominal organs to produce a pattern of symptoms. The difficult evaluations for these conditions have been simplified by the use of abdominal US of the vessels in question.

Median Arcuate Ligament Syndrome

Median arcuate ligament syndrome (MALS), also called the celiac artery compression syndrome and Dunbar syndrome, occurs when the median arcuate ligament compresses the celiac axis and celiac ganglion, typically producing abdominal pain. It was first identified by Harjola in 1963 [22]. The median arcuate ligament connects the right cura and the left cura of the diaphragm, forming the anterior border of the aortic hiatus.

Inexpensive, noninvasive, rapid, and without the risks of contrast and radiation, Doppler ultrasound provides an effective alternative to the angiography and CT-angiography. Two prospective trials in adults comparing the Doppler Ultrasound to the lateral abdominal aortography confirmed the accuracy of this modality in diagnosing the condition. The more recent investigation confirmed 100% sensitivity of the Doppler ultrasound for identifying clinically significant (>70%) celiac artery stenosis. Specificity, positive predictive value, and negative predictive value were 87, 57, and 100%, respectively [23, 24]. A later retrospective analysis on children and adolescents further substantiated the suitability and value of the Doppler ultrasound in diagnosing MALS.

For the examination, patients should fast for a minimum of 8 h prior to the study. Given the vague clinical presentation, the entire mesenteric system should be evaluated. Lower frequency (in the range of 3–7.5 MHz) and harmonic imaging provide clearer images. All velocity measurements should be obtained with angle correction of less than 60° [25]. Wolfman et al. have demonstrated the importance of acquiring both supine and erect Doppler images, noting a tendency of pathological values to normalize when children are positioned erect. The stage of the respiratory cycle dramatically affects the results, with much higher peak velocities observed at peak expiration than peak inspiration due to the dorsal movement of the aorta upon inhalation. One study in adults suggested that 73% of the patients with end-expiration celiac artery stenosis observed via ultrasound demonstrated at least partial resolution of the pathology at end-inspiration [26, 27]. Consensus for the proper moment in the respiratory cycle to examine the patient has not been established, with authors alternatively opting for either the best-case or worst-case ultrasonagraphic results. Examinations require fewer than 20 min for experienced ultrasongraphers to complete.

While normal blood flow velocities for adults and neonates are available, such data are not well-established for children, and no rigorously verified criteria for defining MALS in the pediatric population exist. For adults, prospective studies have shown that peak systolic velocities greater than 200 cm/s in the celiac artery (or no flow detected) correlate with at least 70% stenosis of the vessel, with 75% sensitivity and 89% specificity [25]. Most subsequent publications have adopted these standards, even for children, and have demonstrated their reliability in diagnosing the MALS [24]. The largest series of children with MALS ($n = 59$) entertained more liberal criteria, including greater than twofold acceleration in flow between the aorta and celiac artery, but a lack of confirmatory data prevents us from endorsing this expanded definition. Figure 9.5 illustrates the findings in MALS.

When appropriate, surgical intervention can proceed via either open or laparoscopic means. For either approach, the use of intraoperative ultrasound can confirm the efficacy of the repair and the resolution of the stenosis by showing decreased peak velocities in the celiac artery [28]. Thus, for screening, diagnosis, and post-treatment verification, Doppler ultrasound is a highly effective, inexpensive modality well-suited for the pediatric population.

Superior Mesenteric Artery Syndrome (SMAS)

SMAS (also referred to as Wilkie's disease, cast syndrome, arterial mesenteric duodenal compression) occurs when the SMA and aorta entrap and compress the third portion of the duodenum. It was first noted by Rikitansky in 1842 and

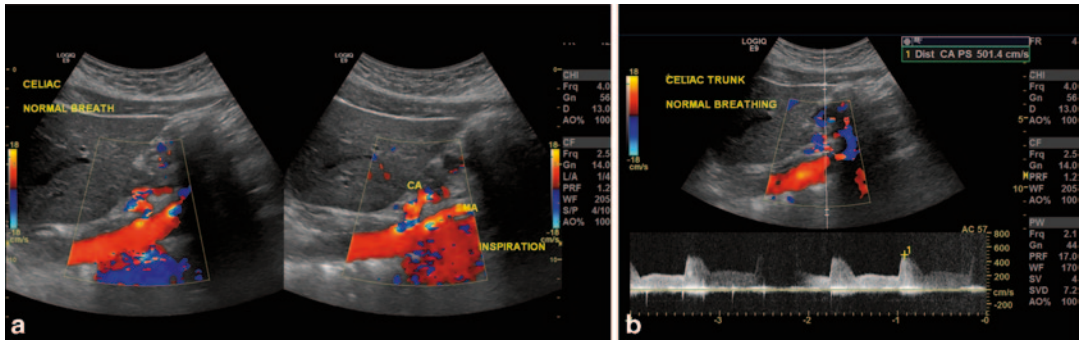

Fig. 9.5 Median arcuate ligament syndrome *(MALS)*. **a** the angle between the celiac axis and the *SMA* is seen and measured erect and supine as well as in deep inspiration. **b** The velocity measured is > 200 cm/s

more completely described by Wilkie in 1927 [29].

Ultrasound has now assumed an important role in screening for the condition. A 2005 controlled prospective study in adults clearly demonstrated the ability of ultrasound to match CT scans in accurately identifying the vascular features of this syndrome [30, 31]. Exams are performed after an overnight fast and during the expiratory phase of respiration. Low MHZ probes provide the best images. There was no significant difference between conducting the exam in the supine or standing positions, although the lateral position was less sensitive.

Ultrasound can help diagnose SMAS by assessing the angle between the aorta and the SMA (Fig. 9.6a and b) as well as the distance from the aorta to the SMA at the level of the duodenum [32]. In adults, these values have been well studied, and while measurements vary, the literature generally considers a normal angle to be between 25 and 60° and a normal distance to be between 10 and 28 mm. These values in children have recently been studied in 205 consecutive pediatric abdominal CT scans in patients presenting without suspicion for SMAS. This series showed the mean angle to be 45.6 ± 19.6° [33]. The few published cases demonstrating the utility of ultrasound to diagnose SMAS in young patients with otherwise unexplainable abdominal pain have used adult measurements [34]. However, the study of 205 pediatric abdominal CT scans revealed

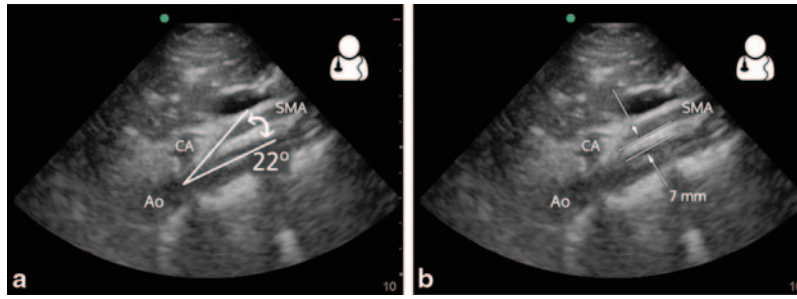

Fig. 9.6 Superior mesenteric artery syndrome *(SMAS)*. A normal aortomesenteric angle is approximately 45°, and an aortomesenteric angle of 6–25° confirms the diagnosis. This angle can be readily measured on ultrasound. **a** To measure the aortomesenteric angle, first obtain a sagittal view of the aorta and delineate landmarks: *Ao*, *CA*, and *SMA*. Measure the *SMA* angle as it takes off from the aorta. **b** A normal aortomesenteric distance is 10–28 mm. An aortomesenteric distance < 8–10 mm suggests *SMA* syndrome in the appropriate clinical setting [32]

that over 20% of the cases demonstrated angles less than 8°—values that meet diagnostic criteria for SMAS, yet the patients denied any symptoms of the syndrome [33]. Moreover, other data show significant inter-operator variability with Doppler measurements of the SMA, challenging the reliability of test. Clearly, clinicians must have a high index of suspicion to evaluate for SMAS and use imaging to confirm clinical assessment rather than solely relying on angles and distances. At present, ultrasound serves well as a screening modality for SMAS, but CT scans ought to be obtained to confirm the diagnosis and clarify the anatomy, particularly if operative intervention is planned.

Nutcracker Syndrome

Nutcracker syndrome refers to an array of symptoms associated with the compression of the LRV. It is crucial to distinguish the syndrome from nutcracker phenomenon, which refers to anatomical and radiological evidence of such constriction without any corresponding symptoms. Anatomists have recognized compression of the LRV between the aorta and SMA since the 1930s [35, 36], but the condition of nutcracker syndrome was not elucidated until the 1970s [37]. Children suffering from the disease report flank and/or abdominal pain, gross hematuria, and varicoceles; some present with asymptomatic proteinuria or microhematuria [38]. Today, ultrasound has an important role in establishing the diagnosis.

Prior to ultrasound, renal venography with pressure gradients established the presence of the disease, with pressure differentials of greater than 3 mm Hg between the LRV and vena cava confirming the disease. This methodology remains the gold-standard, if rarely implemented. (Normal pressure differentials in children have not been established, forcing clinicians to rely on adult parameters). The invasiveness, radiation, and contrast load, not to mention cost, render this technique unappealing, especially in children. In 1986, Wolfish et al. proposed using ultrasound as an alternative [39]. Specifically, they suggested a 50% increase in the diameter of the LRV between the renal hilum and the aorta compared to the segment between the aorta and vena cava reflected compression. The first recorded case of the nutcracker syndrome diagnosed by ultrasound occurred in 1988 in Japan using Wolfish's criteria [40]. Further Japanese studies established clear guidelines for the diagnoses nutcracker phenomenon based on LRV dilation ratios [41, 42], but additional investigation revealed normal LRV diameter varied too much in children to rely on it for diagnostic purposes [43, 44].

The advent of Doppler technology offered a new option in measuring blood flow. However, the anatomy of pediatric patients complicated its initial deployment. With a very short LRV that runs almost perfectly horizontal, children challenged the acquisition of acceptable Doppler angles [45]. As such, early Doppler investigations relied on the identification of the collateral veins to diagnose nutcracker phenomenon, which had a relatively low sensitivity (78%) but 100% specificity when observed [46, 47]. Rarely found on CT scans, Doppler-identified collateral veins remain useful in confidently diagnosing nutcracker phenomenon.

More recently, Doppler-acquired flow velocities have demonstrated reliability and accuracy in identifying the nutcracker phenomenon. With the advent of new technology and the introduction of techniques like instructing patients to drink water prior to the exam (thus eliminating bowel gas and creating clearer windows), Doppler exams became more feasible. A 1996 South Korean study compared Doppler ultrasound directly to LRV pressure gradient measurements in adult patients with the nutcracker syndrome verses controls and found significant differences in the peak velocity of blood flowing in the LRV between the vena cava/aorta and aorta/hilum [48]. The ratio of velocity differences Kim elucidated has since become the foundation of Doppler-diagnosed nutcracker phenomenon. Subsequent investigators

worked to apply these findings to children [49], and in 2001, the first child was diagnosed with the nutcracker syndrome based on this ratio [50].

Since Kim et al. established the ratio, other groups have worked to refine the value and apply it to children. Kim et al. established the cut off ratio for adults to be 5.0 [50]. Pediatric studies have suggested ratios ranging from 4.1 to 4.8, with sensitivities of 100 % and specificities ranging in the low 90s [51–53]. These ratios have proven accurate enough and are so widely accepted that physicians reporting continued use of other modalities like MRA and CT-A scans have been criticized in the literature [54]. Which exact number to use remains debatable, and the ethnic homogeneity of all subjects in these studies is less than ideal, but the repeatability of the results and the relatively narrow range of ratios strongly substantiate the methodology. More recent investigations have also looked to the measuring the aorta–SMA angle as an adjunct to help diagnose nutcracker phenomenon, but given (a) the high sensitivity and specificity of ratios; (b) the dependence of the angle on child positioning; and (c) the aforementioned wide variability of this angle in children, clinicians need not pursue this additional measurement.

Several well-controlled studies have clearly demonstrated the ability of Doppler ultrasound to diagnose nutcracker phenomenon in children by comparing the peak velocities of blood flow in different segments of the LRV. Ultrasound provides a welcome advance from the invasive, expensive, radioactive methods of the 1980s, and, based on the above investigations, can be used exclusively to diagnose the LRV compression characteristic of the nutcracker syndrome.

Stenosis, Aneurysm, Collaterals, and Thrombosis

Renal Artery Stenosis

Ultrasound can be used to evaluate the causes of renovascular hypertension, specifically renal artery stenosis, often induced by Takayasu's arteritis in children [55]. Typically, the patient is placed in a lateral decubitus position, with an angle of insonation of about 60°. A velocity in the renal artery > 200 m/s is consistent with renal artery stenosis, and a difference in the resistive indices > 0.05 between the two kidneys with the lower resitive index (RI) being on the side of the kidney with the elevated velocities is consistent with renal artery stenosis of > 60 %.

Aneurysms

Abdominal aneurysms are uncommon in children and most often occur with Kawasaki's disease [56], pancreatitis [57], or after trauma to the liver and spleen [58]. Ultrasound can be used to evaluate for pseudoaneurysm or true aneurysm and is a useful technique to monitor success after intervention. Ultrasound can reliably measure the dimensions of the aneurysm and characterize the flow of blood in the lesion.

Collaterals and Portosystemic Shunts

Portal hypertension is caused by a number of conditions that create an increase in the PV pressure. These are generally classified as pre-hepatic, post-hepatic, or sinusoidal (intra-hepatic). There are a number of physiologic sequelae to prolonged portal hypertension. In pediatric surgery, pre-hepatic causes can be due to PV thrombosis after umbilical vein catheterization (although more often from unclear etiology). If portal hypertension progresses, appropriate flow can become hepatofugal in direction, and ultimately there is shunting of portal blood flow to the systemic veins that return blood to the heart via the inferior vena cava. Ultrasound can be used to document and follow shunts and collaterals that develop in patients with the chronic portal hypertension. Ultrasound can demonstrate changes in flow through portosystemic shunts [59], along with changes in the characteristics of flow (i.e.,

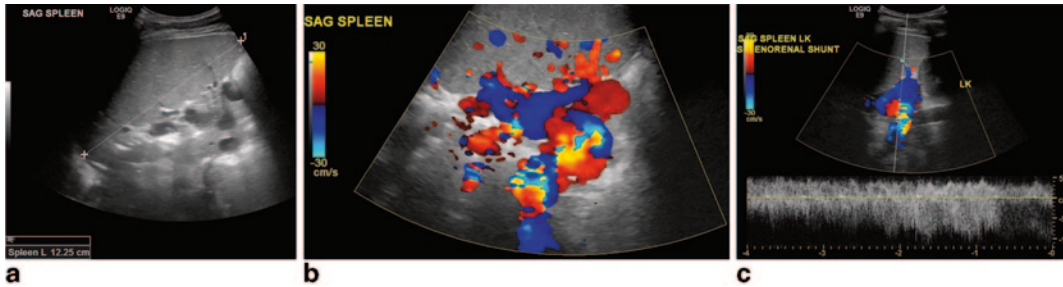

Fig. 9.7 Splenorenal shunt. **a** Ultrasound identifies the dilated vessels at the splenic hilum and documents the splenomegaly. **b** Hepatopetal flow identified in the splenic parenchyma. **c** Close proximity of flow between the liver and kidney, patent renal vein

reliably demonstrative of loss of variation with respiration or changes in Doppler waveform patterns).

As an example, Fig. 9.7 demonstrates a splenorenal shunt. In the top panel, the spleen is measured and noted to be enlarged with normal parenchyma. The tortuous splenic collaterals are seen at the hilum. In the middle panel, the central PV is not identified. However, hepatopedal (appropriate directional) portal venous flow is detected within the parenchyma. The hepatic veins demonstrate gross patency. In the bottom panel, the limited image of the left kidney demonstrates no abnormality. Flow is toward the kidney, compatible with a splenorenal shunt. This is patent and demonstrates flow above and below the baseline. Peak velocity ranges between 50 and 100 cm/s. The main renal vein is grossly patent.

Thrombosis

Duplex sonography is the main radiographic method for detecting and monitoring thrombosis of the larger veins. All major veins can be easily visualized and examined for flow characteristics except the superior vena cava (SVC) and the more distal SMV, which are often obscured by air from lungs or bowel. To evaluate the SVC, MRA, or venous phase CTA are needed for optimal evaluation. Clinically, thrombosis is common in the femoral, iliac, internal jugular, and subclavian veins, mostly secondary to central venous catheters [60] (Fig. 9.8). Extent and resolution after anticoagulation therapy is preferably monitored with the ultrasound, which can even be performed as a bedside study in the intensive care unit (Fig. 9.9). Ultrasound-guided placement of vena cava filters is standard of care in many centers for adolescents with increased risk of peripheral deep venous thrombosis to prevent a large pulmonary embolus [63]. The exact position for deployment just inferior to the confluence with the renal veins is paramount when placing these devices (Fig. 9.10).

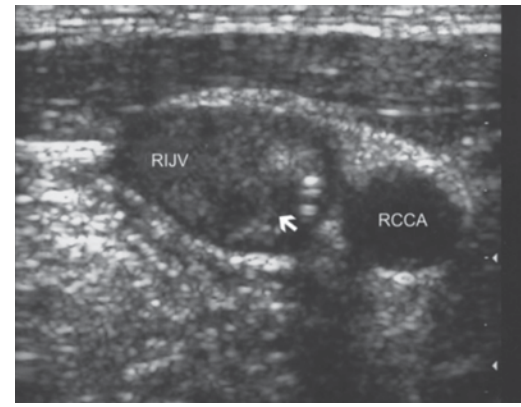

Fig. 9.8 Thrombus visualized within the right internal jugular vein *(RIJV) (arrow)*. The vessel could not be compressed. *RCCA* right common carotid artery [61]

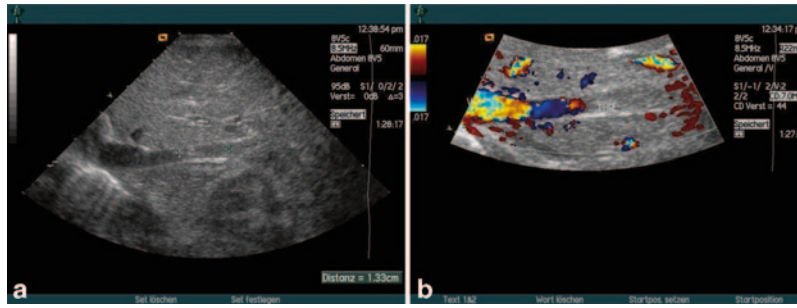

Fig. 9.9 Newborn 36th gestational week with massive swelling of abdomen and thorax. The extremities were only mildly edematous. **a** Depiction of an echogenic thrombus in the area of the middle inferior vena cava at about the level of the renal vein junction. The increased echogenicity of the thrombus indicates that the clot is at least 7 days old. **b** The color Doppler shows that the retrohepatic inferior vena cava above the level of the thrombus *(THR)* is patent without any clot burden [62]

Summary

Ultrasonography of abdominal vessels aids in the workup of many abdominal conditions in children. Simple to employ with no risks to the patient, ultrasound has become a very important implement in the physician's armamentarium for diagnostic workup and management decisions involving the major vessels. Every abdominal organ, their vascular supply, and the large central vessels are able to be imaged with ultrasound, making it a very versatile tool. Color Doppler can picture and quantify pathology within the vasculature itself. As ultrasound involves no contrast or radiation and is noninvasive and repeatable, it is a logical study to be included in the workup of the many diagnoses involving the abdominal vasculature.

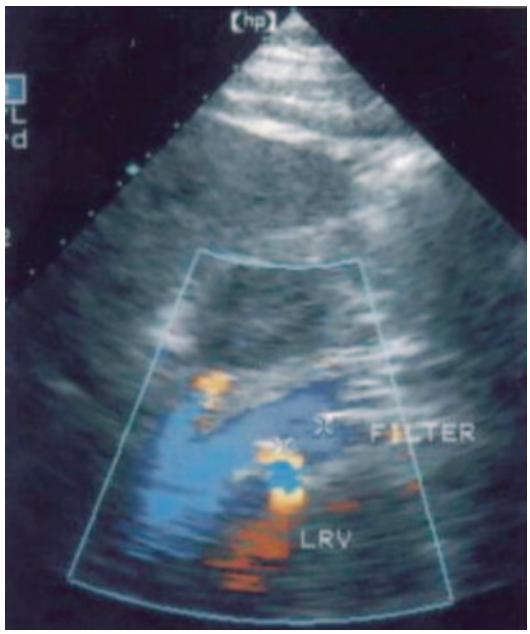

Fig. 9.10 Color-flow duplex ultrasound scan with patent *IVC* with tip of Greenfield filter seen just distal to the *LRV*. The patient is scanned from the right flank while in left decubitus position. The head of the patient is to the left [63]

References

1. Epelman M. The whirlpool sign. Radiology. 2006;240(3):910–1.
2. Applegate KE. Evidence-based diagnosis of malrotation and volvulus. Pediatr Radiol. 2009;39:161–3.
3. Stephens LR, Donoghue V, Gillick J. Radiological versus clinical evidence of malrotation, a tortuous tale–10-year review. Eur J Pediatr Surg. 2012;22(3):238–42.
4. Chao H-C, Kong M-S, Chen J-Y, Lin S-J, Lin J-N. Sonographic features related to volvulus in neonatal intestinal malrotation. J Ultrasound Med. 2000;19(6):371–6.
5. Gaines P, Saunders A, Drake D. Midgut malrotation diagnosed by ultrasound. Clin Radiol. 1987;38(1):51–3.
6. Loyer E, Eggli KD. Sonographic evaluation of superior mesenteric vascular relationship in malrotation. Pediatr Radiol. 1989;19(3):173–5.

7. Weinberger E, Winters W, Liddell R, Rosenbaum D, Krauter D. Sonographic diagnosis of intestinal malrotation in infants: importance of the relative positions of the superior mesenteric vein and artery. AJR Am J Roentgenol. 1992;159(4):825–8.
8. Zerin JM, DiPietro M. Superior mesenteric vascular anatomy at US in patients with surgically proved malrotation of the midgut. Radiology. 1992;183(3):693–4.
9. Dufour D, Delaet M, Dassonville M, Cadranel S, Perlmutter N. Midgut malrotation, the reliability of sonographic diagnosis. Pediatr Radiol. 1992;22(1):21–3.
10. Pracros J, Sann L, Genin G, Tran-Minh V, de Finfe CM, Foray P, et al. Ultrasound diagnosis of midgut volvulus: the "whirlpool" sign. Pediatr Radiol. 1992;22(1):18–20.
11. Shimanuki Y, Aihara T, Takano H, Moritani T, Oguma E, Kuroki H, et al. Clockwise whirlpool sign at color Doppler US: an objective and definite sign of midgut volvulus. Radiology. 1996;199(1):261–4.
12. Patino MO, Munden MM. Utility of the sonographic whirlpool sign in diagnosing midgut volvulus in patients with atypical clinical presentations. J Ultrasound Med. 2004;23(3):397–401.
13. Yeh WC, Wang HP, Chen C, Wang HH, Wu MS, Lin JT. Preoperative sonographic diagnosis of midgut malrotation with volvulus in adults: the "whirlpool" sign. J Clin Ultrasound. 1999;27(5):279–83.
14. Van Winckel M, Voet D, Robberecht E. "Whirlpool sign": not always associated with volvulus in intestinal malrotation. J Clin Ultrasound. 1996;24(7):367–70.
15. Marine MB, Karmazyn B. Imaging of malrotation in the neonate. Semin Ultrasound CT MR. 2014;35(6):555–70.
16. Applegate KE, Anderson JM, Klatte EC. Intestinal malrotation in children: a problem-solving approach to the upper gastrointestinal series. Radiographics. 2006;26(5):1485–500.
17. Yousefzadeh DK. The position of the duodenojejunal junction: the wrong horse to bet on in diagnosing or excluding malrotation. Pediatr Radiol. 2009;39(2):172–7.
18. Orzech N, Navarro OM, Langer JC. Is ultrasonography a good screening test for intestinal malrotation? J Pediatr Surg. 2006;41(5):1005–9.
19. Esposito F, Vitale V, Noviello D, Serafino MD, Vallone G, Salvatore M, et al. Ultrasonographic Diagnosis of midgut volvulus with malrotation in children. J Pediatr Gastroenterol Nutr. 2014;59(6):786–8.
20. Quail MA. Question 2 is Doppler ultrasound superior to upper gastrointestinal contrast study for the diagnosis of malrotation? Arch Dis Child. 2011;96(3):317–8.
21. Ashley LM, Allen S, Teele RL. A normal sonogram does not exclude malrotation. Pediatr Radiol. 2001;31(5):354–6.
22. Harjola PT. A rare obstruction of the coeliac artery. Report of a case. Ann Chir Gynaecol Fenn. 1963;52:547–50.
23. Aschenbach R, Basche S, Vogl TJ. Compression of the celiac trunk caused by median arcuate ligament in children and adolescent subjects: evaluation with contrast-enhanced MR angiography and comparison with Doppler US evaluation. J Vasc Interv Radiol. 2011;22(4):556–61.
24. Moneta GL, Yeager RA, Dalman R, Antonovic R, Hall LD, Porter JM. Duplex ultrasound criteria for diagnosis of splanchnic artery stenosis or occlusion. J Vasc Surg. 1991;14(4):511–20.
25. Lynch K. Celiac artery compression syndrome a literature review. J Diagn Med Sonogr. 2014;30(3):143–8.
26. Wolfman D, Bluth EI, Sossaman J. Median arcuate ligament syndrome. J Ultrasound Med. 2003;22(12):1377–80.
27. Papacci P, Giannantonio C, Cota F, Latella C, Semeraro CM, Fioretti M, et al. Neonatal colour Doppler ultrasound study: normal values of abdominal blood flow velocities in the neonate during the first month of life. Pediatr Radiol. 2009;39(4):328–35.
28. Moneta GL, Lee RW, Yeager RA, Taylor LM, Porter JM. Mesenteric duplex scanning: a blinded prospective study. J Vasc Surg. 1993;17(1):79–86.
29. Roayaie S, Jossart G, Gitlitz D, Lamparello P, Hollier L, Gagner M. Laparoscopic release of celiac artery compression syndrome facilitated by laparoscopic ultrasound scanning to confirm restoration of flow. J Vasc Surg. 2000;32(4):814–7.
30. Kohn GP, Bitar RS, Farber MA, Marston WA, Overby DW, Farrell TM. Treatment options and outcomes for celiac artery compression syndrome. Surg Innov. 2001;18(4):338–43.
31. Wilkie D. Chronic duodenal ileus. Am J Med Sci. 1927;173(5):643–8.
32. Neri S, Signorelli S, Mondati E, Pulvirenti D, Campanile E, Di Pino L, et al. Ultrasound imaging in diagnosis of superior mesenteric artery syndrome. J Intern Med. 2005;257(4):346–51.
33. Unal B, Aktas A, Kemal G, Bilgili Y, Guliter S, Daphan C, et al. Superior mesenteric artery syndrome: CT and ultrasonography findings. Diagn Interv Radiol. 2005;11(2):90–5. http://www.ultrasoundoftheweek.com/uotw-21-answer/.
34. Arthurs O, Mehta U, Set P. Nutcracker and SMA syndromes: what is the normal SMA angle in children? Eur J Radiol. 2012;81(8):e854–e61.
35. Abu-Zidan F, Hefny A, Saadeldinn Y, El-Ashaal Y. Sonographic findings of superior mesenteric artery syndrome causing massive gastric dilatation in a young healthy girl. Singapore Med J. 2010;51(11):e184–6.
36. Chin L-W, Chou M-C, Wang H-P. Ultrasonography diagnosis of superior mesenteric artery syndrome in the ED. Am J Emerg Med. 2005;25:864.e5–.e6.

37. Fagarasanu I. Recherches anatomiques sur la veine renale gauche et ses collaterales; leurs rapports avec la pathogenie du varicocele essential et des varices du ligament large. (Demonstrations experimentales). Ann Anat Pathol. 1938;15:9–52.
38. Grant J. Method of anatomy. Baltimore: Williams and Wilkins; 1938. p. 1.
39. De Schepper A. " Nutcracker" phenomenon of the renal vein and venous pathology of the left kidney. J Belge Radiol. 1971;55(5):507–11.
40. Alaygut D, Bayram M, Soylu A, Cakmakcı H, Türkmen M, Kavukcu S. Clinical course of children with nutcracker syndrome. Urology. 2013;82(3): 686–90.
41. Wolfish N, McLaine P, Martin D. Renal vein entrapment syndrome: frequency and diagnosis. A lesson in conservatism. Clin Nephrol. 1986;26(2):96–100.
42. Arima M, Hosokawa S, Ogino T, Ihara H, Terakawa T, Ikoma F. Ultrasonographically demonstrated nutcracker phenomenon: alternative to angiography. Int Urol Nephrol. 1990;22(1):3–6.
43. Okada M, Tsuzuki K, Ito S. Diagnosis of the nutcracker phenomenon using two-dimensional ultrasonography. Clin Nephrol. 1998;49(1):35–40.
44. Takahashi Y, Sano A, Matsuo M. An ultrasonographic classification for diverse clinical symptoms of pediatric nutcracker phenomenon. Clin Nephrol. 2005;64(1):47–54.
45. Zerin J, Hernandez R, Sedman A, Kelsch R. "Dilatation" of the left renal vein on computed tomography in children: a normal variant. Pediatr Radiol. 1991;21(4):267–9.
46. Buschi AJ, Harrison RB, Norman A, Brenbridge A, Williamson B, Gentry R, et al. Distended left renal vein: CT/sonographic normal variant. Am J Roentgenol. 1980;135(2):339–42.
47. Park SJ, Shin JI. Renal Doppler ultrasonography in the diagnosis of nutcracker syndrome. Eur J Pediatr. 2013;172(1):135–6.
48. Stavros AT, Sickler KJ, Menter RR. Color duplex sonography of the nutcracker syndrome (aortomesenteric left renal vein compression). J Ultrasound Med. 1994;13(7):569–74.
49. Takebayashi S, Ueki T, Ikeda N, Fujikawa A. Diagnosis of the nutcracker syndrome with color Doppler sonography: correlation with flow patterns on retrograde left renal venography. Am J Roentgenol. 1999;172(1):39–43.
50. Kim SH, Cho SW, Kim HD, Chung JW, Park JH, Han MC. Nutcracker syndrome: diagnosis with Doppler US. Radiology. 1996;198(1):93–7.
51. Cho BS, Choi YM, Kang HH, Park SJ, Lim JW, Yoon TY. Diagnosis of nut-cracker phenomenon using renal Doppler ultrasound in orthostatic proteinuria. Nephrol Dial Transplant. 2001;16(8): 1620–5.
52. Kavukcu S, Kasap B, Göktay Y, Seçil M. Doppler sonographic indices in diagnosing the nutcracker phenomenon in a hematuric adolescent. J Clin Ultrasound. 2004;32(1):37–41.
53. Cheon J-E, Kim WS, Kim I-O, Kim SH, Yeon KM, Ha IS, et al. Nutcracker syndrome in children with gross haematuria: Doppler sonographic evaluation of the left renal vein. Pediatr Radiol. 2006;36(7):682–6.
54. Shin JI, Park JM, Lee JS, Kim MJ. Effect of renal Doppler ultrasound on the detection of nutcracker syndrome in children with hematuria. Eur J Pediatr. 2007;166(5):399–404.
55. Shin JI, Park JM, Lee JS, Kim MJ. Doppler ultrasonographic indices in diagnosing nutcracker syndrome in children. Pediatr Nephrol. 2007;22(3): 409–13.
56. Park SJ, Oh JY, Shin JI. Diagnostic value of renal Doppler ultrasonography for detecting nutcracker syndrome in children with recurrent gross hematuria. Clin Pediatr (Phila). 2012;51(10):1001-.
57. TA L, Gajjar P, McCulloch M, Scott C, Numanoglu A, Nourse P. Impact of revascularization on hypertension in children with Takayasu's arteritis-induced renal artery stenosis: a 21-year review. Pediatr Nephrol. 2015. Feb 4.
58. Hoshino S, Tsuda E, Yamada O. Characteristics and fate of systemic artery aneurysm after Kawasaki disease. J Pediatr. 2015;167:108–12.e2.
59. Puri A, Acharya H, Tyagi S, Curian S, Chadha R, Anand R, Choudhary SR. Pseudoaneurysm of the radial branch of the splenic artery with pancreatic pseudocyst in a child with recurrent acute pancreatitis: treatment with endovascular stent graft and cystogastrostomy. J Pediatr Surg. 2012;47(5):1012–5.
60. Safavi A, Beaudry P, Jamieson D, Murphy JJ. Traumatic pseudoaneurysms of the liver and spleen in children: is routine screening warranted? J Pediatr Surg. 2011;46(5):938–41.
61. Pinter SZ, Rubin JM, Kripfgans OD, Novelli PM, Vargas-Vila M, Hall AL, Fowlkes JB. Volumetric blood flow in transjugular intrahepatic portosystemic shunt revision using 3-dimensional Doppler sonography. J Ultrasound Med. 2015;34(2):257–66.
62. Shah SH, West AN, Sepanski RJ, Hannah D, May WN, Anand KJ. Clinical risk factors for central line-associated venous thrombosis in children. Front Pediatr. 2015;3:35.
63. Karakitsos D, Labropoulos N, De Groot E, Patrianakos AP, Kouraklis G, Poularas J, et al. Real-time ultrasound-guided catheterisation of the internal jugular vein: a prospective comparison with the landmark technique in critical care patients. Crit Care. 2006;10(6):R162. http://www.radiologyteacher.com/index.cgi?&nav=view&DatID=95.
64. Cahn MD, Rohrer MJ, Martella MB, Cutler BS. Long-term follow-up of Greenfield inferior vena cava filter placement in children. J Vasc Surg. 2001;34(5):820–5.